Research Square

Preprints are preliminary reports that have not undergone peer review.
They should not be considered conclusive, used to inform clinical practice,
or referenced by the media as validated information.

Prediction of Lymphovascular Invasion in Breast Cancer Using Intratumoral and Peritumoral MRI Radiomics Models Based on DCE-MRI: A Multicenter Study

Hongen Li
Guangdong Women and Children Hospital
Yihui Zeng
Guangdong Women and Children Hospital
Qingwen Xiao
First Affiliated Hospital of Jinan University
Jianbin Tan
Guangdong Women and Children Hospital
Yan Zhang
doctorzhangyan@vip.163.com
Guangdong Women and Children Hospital

Article

Keywords:

Posted Date: November 12th, 2026

DOI: https://doi.org/10.21203/rs.3.rs-11462010/v1

License: This work is licensed under a Creative Commons Attribution 4.0 International License.
Read Full License

Additional Declarations: No competing interests reported.

Prediction of Lymphovascular Invasion in Breast Cancer Using Intratumoral and Peritumoral MRI Radiomics Models Based on DCE-MRI: A Multicenter Study

Hongen Li, BS[*1] • *Yihui Zeng, BS*[*1] • *Qingwen Xiao, MS*[2] • *Jianbin Tan, MS*[1] • *Yan Zhang, MS*[1,+]

[*]H.L. and Y.Z. (Yihui Zeng) contributed equally to this work

Author affiliations:

[1]Department of Radiology, Guangdong Women and Children Hospital, No. 521 Xingnan Avenue, Panyu District, Guangzhou 511442, China

[2]The First Affiliated Hospital of Jinan University, Guangzhou, China

[+]**Corresponding author:** Y.Z. (Yan Zhang) (Email: doctorzhangyan@vip.163.com)

[Abstract] Purpose This study explores the predictive value of intramural and peritumoral radiomics features based on dynamic contrast-enhanced magnetic resonance imaging (DCE-MRI) for lymphovascular invasion (LVI) in breast cancer. It compares the predictive efficacy of different peritumoral regions and feature fusion methods, and constructs a combined prediction model integrating clinical characteristics. **Materials and Methods** Retrospectively collected images from 757 breast cancer patients with pathologically confirmed diagnoses who underwent breast DCE-MRI examinations at two medical centers. Data from Center 1 served as the training set (n=529), while data from Center 2 formed the external validation set (n=228). Tumor lesions were semi-automatically delineated using ITK-SNAP software, with peritumoral regions automatically expanded. Regions of interest (ROIs) were selected on the maximum intensity phase of DCE-MRI. Radiomics features were extracted using PyRadiomics across four modalities: intratumoral, peritumoral (1mm, 3mm, 5mm, 7mm, 10mm, 15mm, 20mm), Tumor+Peri7mm, and ImageFusion7 (a fusion of tumor and optimal 7mm peritumoral regions). Data dimensionality reduction and feature selection were performed using Spearman correlation analysis, Least Absolute Shrinkage and Selection Operator (LASSO) regression, and Maximum Relevance-Minimum Redundancy (mRMR) methods. Five classifiers—support vector machine (SVM), extreme trees (ET), extreme gradient boosting (XGBoost), light gradient boosting machine (LightGBM), and multilayer perceptron (MLP)—were evaluated under different feature models to identify the optimal classifier for constructing the radiomics model. Clinical Features: Single- and multi-factor logistic regression screened clinical risk factors to construct a clinical model. Comprehensive evaluations were conducted on the clinical model, the optimal radiomic model, and a combined model incorporating clinical features with optimal radiomic features. Receiver operating characteristic (ROC) curves analyzed predictive performance, with area under the curve (AUC) calculated. A fusion model was established by integrating the radiomic score (rad-score) from the highest-performing predictive model and visualized via a nomogram. The clinical utility of the predictive models was assessed using calibration curves and decision curve analysis (DCA). **Results** Clinical

characteristics: The AUC values of the clinical model based on histological grade, sentinel lymph node status, and TIC were 0.738 (95% CI: 0.6949 - 0.7802) and 0.749 (95% CI: 0.6830 - 0.8141) in the training and validation sets, respectively. As a key indicator reflecting lymph node metastasis in primary tumors, sentinel lymph node status is widely recognized for its role in breast cancer staging and prognostic assessment. For instance, in breast cancer, the area under the ROC curve for a non-sentinel lymph node metastasis risk prediction model in sentinel lymph node-positive patients reached 0.7613, demonstrating its clinical utility. Radiomics: Among the various peritumoral models, the 7 mm peritumoral model demonstrated the best performance. Results indicate that the radiomics model based on the ImageFusion7 (intra-tumor and peritumoral image fusion region) demonstrated optimal diagnostic performance, with the XGBoost classifier showing particularly outstanding results: an AUC of 0.861 (95% CI: 0.8302 - 0.8914) in the training set and an AUC of 0.709 (95% CI: 0.6407 - 0.7768). When constructing a clinical-imaging fusion model, the ROC curve based on clinical features and Radscore values achieved AUC values of 0.892 (95% CI: 0.8629 - 0.9165) and 0.778 (95% CI: 0.7140 - 0.8375) in the training and validation sets, respectively, surpassing all single models and the intra-tumoral/peritumoral model. The DCA curve demonstrated that the combined model exhibited the highest clinical efficacy and closely followed the diagonal line in the calibration curve, indicating superior model fit and generalization capability. **Conclusions** An image-based model utilizing DCE-MRI effectively predicts lymphovascular invasion (LVI) status in breast cancer, with the ImageFusion7 model—which integrates images from both the tumor interior and a 7mm peritumoral region—demonstrating optimal predictive performance. Combining this model with clinically independent risk factors further enhances its accuracy. The constructed fusion model exhibits strong discriminatory power and clinical applicability, providing a valuable tool for non-invasive preoperative assessment of LVI risk.
【Keywords】 Breast cancer; Vascular invasion; Peritumoral region; Magnetic resonance imaging; Radiomics; Histogram

Globally, breast cancer has become the most common malignant tumor among women [1]. According to projections by the International Agency for Research on Cancer (IARC) for 2025, new breast cancer cases worldwide will increase by 38% and deaths will rise by 68% over the next 25 years [2]. Radical surgery remains the primary treatment modality for breast cancer[2], yet patients commonly face tumor recurrence and metastasis postoperatively. Lymphovascular invasion (LVI), also known as lymphovascular invasion, refers to the presence of tumor cells within distinct endothelial spaces (lymphatic vessels or blood vessels) in the surrounding spaces of invasive breast cancer [3-4], and/or the involvement of peritumoral lymphatic spaces or blood vessels by cancer emboli [5]. Studies indicate that LVI is widely recognized as a poor prognostic factor for invasive breast cancer (IBC) [6-7]. The College of American Pathologists (CAP) considers LVI assessment the "gold standard" for cancer reporting. However, needle biopsy sometimes fails to reflect the tumor's complete histopathological picture, leading to diagnostic delays. Consequently,

identifying an effective tool for accurately predicting vascular invasion preoperatively is particularly crucial. Magnetic resonance imaging (MRI) holds significant value in diagnosing and evaluating breast cancer characteristics due to its high soft tissue resolution and temporal continuity [8-9]. Traditional MRI-based morphological studies, such as the perivascular sign, kinetic enhancement curves, peritumoral edema, tumor apparent diffusion coefficient (ADC), and tumor ADC, have been closely associated with LVI [10-11]. However, these methods exhibit certain limitations in diagnostic performance. Radiomics employs high-throughput analysis of medical images to generate quantitative information, then constructs descriptive or predictive models of tumor characteristics based on selected features to achieve preoperative diagnosis [12-13]. Previous radiomics studies have predominantly focused on extracting information from within the tumor, often neglecting the peritumoral region [14-15]. When addressing peritumoral regions, researchers typically treat the tumor and surrounding areas as two independent regions of interest (ROIs) for feature extraction [16-17]. In contrast, this study treats both intra-tumoral and peritumoral regions as a unified ROI for radiomics feature extraction, while also separately extracting intra- and peritumoral features. The optimal ROI pattern is selected through comparative analysis. This study aims to extract radiomics features from four ROI patterns, construct multivariate models using five distinct machine learning methods, and compare their performance. A fusion model integrating clinical imaging and radiomics features is proposed, demonstrating the best performance in predicting lymphovascular invasion (LVI) in breast cancer.

1 Materials and Methods

1.1 Clinical Data

This study adheres to the Declaration of Helsinki.This retrospective study was approved by the Medical Ethics Committee of Guangdong Women and Children Hospital (Approval No.: Guangdong Women and Children Hospital Medical Ethics No. [20261015]) and the Scientific Research Ethics Committee of the First Affiliated Hospital of Jinan University (Approval No.: KY-2026-109). The requirement for informed consent was waived by both ethics committees due to the retrospective nature of the study.

This retrospective study included 757 patients with pathologically confirmed breast cancer who underwent breast MRI prior to surgery. Among them, 529 patients from Center 1 were assigned to the training cohort, while 228 patients from Center 2 were assigned to the external validation cohort. The patient enrollment process is illustrated in Figure 1.

Between September 2021 and October 2025, this retrospective study enrolled breast cancer patients who underwent preoperative MRI examinations at two centers. Inclusion criteria were: ① Postoperative pathology confirming primary breast cancer with assessed lymphovascular invasion (LVI) status; ② Breast MRI performed within 2 weeks preoperatively, including dynamic contrast-enhanced MRI (DCE-MRI) sequences; ③ No interventional diagnostic or therapeutic procedures prior to MRI. Exclusion criteria: ① Postoperative pathology specimens failing to clarify vascular/lymphatic invasion status; ② Patients receiving radiotherapy or

chemotherapy for breast or other tumors prior to surgery; ③ Incomplete clinical, pathological, or imaging data. The final cohort comprised 757 female patients aged 24–81 years (mean 50.17 ± 10.38 years).

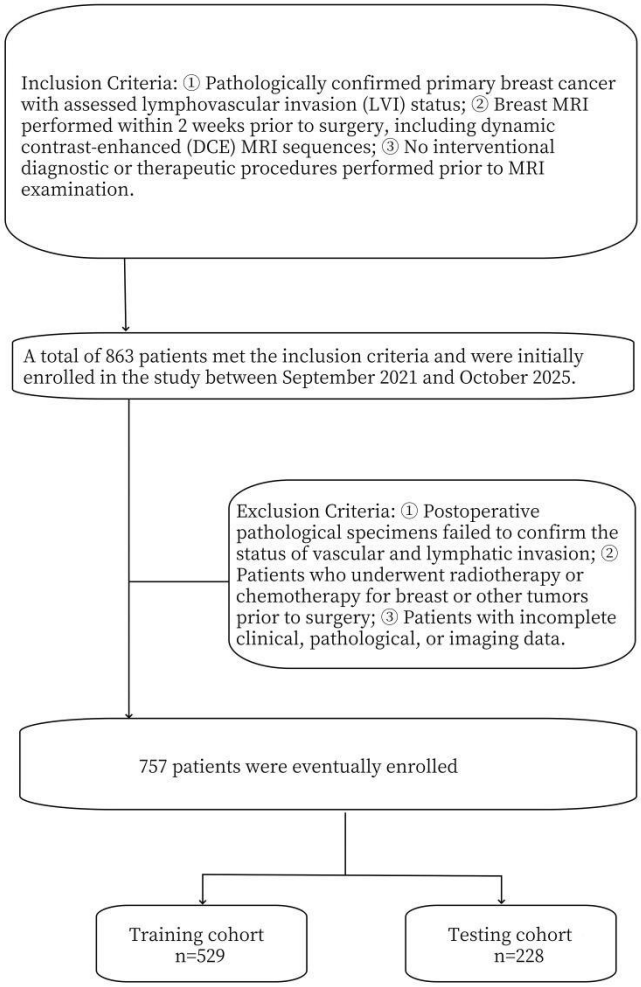


Fig 1. Patient Enrollment Flowchart

1.2 Inspection Methods

Using a Philips Ingenia 3.0T MRI scanner from the Netherlands with a 16-channel phased array coil specifically designed for breast imaging. Specific scanning sequences and parameters are as follows: ① Transverse T1-weighted imaging (T1WI): Repetition time (TR) 400–600 ms, Echo time (TE) 8 ms, Slice thickness 4 mm, Slice spacing 0.4 mm, Number of slices 40, Matrix 212×240, Field of view (FOV) 200 mm ×320 mm, Number of echo planes (NEX) 1; ② Fat-suppressed transverse T2-weighted imaging (T2WI): TR 3000–5,000 ms, TE 75 ms, slice thickness 4 mm, slice spacing 0.4 mm, 40 slices, matrix 192×221, FOV 190 mm×339 mm, NEX 1; ③ Diffusion-weighted imaging (DWI) in the transverse plane: TR 6,550 ms, TE 99 ms, slice thickness 4 mm, slice spacing 0.4 mm, number of slices 40, matrix 212×142, FOV 400 mm×340 mm, NEX 1, b-values 0 and 800 s/mm²; ④ Transverse dynamic contrast-enhanced MRI (DCE-MRI): TR 4.4 ms, TE 2.2 ms, slice thickness 1.6 mm, slice spacing -0.8 mm, number of slices 187, matrix 328×392, FOV 280 mm×339 mm, NEX=1. The contrast agent used was gadoteric acid glucamine injection (National Drug Approval Number H20153167), administered intravenously at 0.2 mmol/kg body weight with an infusion rate of 2.0

ml/s, followed by 15 ml of saline at the same rate. A total of 6 time-phase contrast-enhanced images were acquired.

1.3 Clinical Pathology and MRI Semantic Feature Evaluation

In the absence of known pathological findings, two associate chief radiologists with over 10 years of breast imaging diagnostic experience independently evaluated the MRI images, ensuring professional and accurate assessment. In cases of disagreement, consensus was reached through consultation with a third senior radiologist (experience >20 years). The MRI semantic features evaluated included: breast glandular density (dense vs. non-dense), time-intensity curve (TIC) pattern [influx (Type I), plateau (Type II), efflux (Type III)], MRI-assessed axillary lymph node status (positive vs. negative), and MRI-measured tumor maximum diameter (2 cm vs. ≥2 cm).

Determination of vascular invasion: Under light microscopy, clusters of cancer cells are visible within the spaces surrounded by flattened endothelial cells, and these clusters are in continuity with the flattened endothelial cells.

Clinical and pathological characteristics significantly influence breast cancer prognosis, including age, menopausal status, family history of breast cancer, histological grade, sentinel lymph node status, and biological markers. Biological markers primarily include estrogen receptor (ER), progesterone receptor (PR), human epidermal growth factor receptor 2 (HER-2), and cell proliferation index (Ki-67). ER and PR assessment criteria: <1% positive nuclei are considered negative, ≥1% are positive. HER-2 assessment criteria: Scores of "-" or "+" are negative; "+++" is positive. Scores of "++" require further fluorescence in situ hybridization (FISH) testing, where gene amplification indicates positive status and no amplification indicates negative status. Ki-67 assessment criteria: ≥14% is high expression; <14% is low expression. According to the 2013 St. Gallen International Breast Cancer Conference consensus [18], breast cancer molecular subtypes are clearly defined into four categories: Luminal A (ER/PR-positive, HER2-negative, low Ki-67 expression), Luminal B (further subdivided into HER2-negative and HER2-positive subtypes), HER2-overexpressing (HER2-positive, ER and PR-negative), and triple-negative (ER, PR, and HER2 all negative).

1.4 Radiomics Analysis Process

The workflow of radiomics encompasses image segmentation, feature extraction, feature selection, model building, and validation (Figure 2).

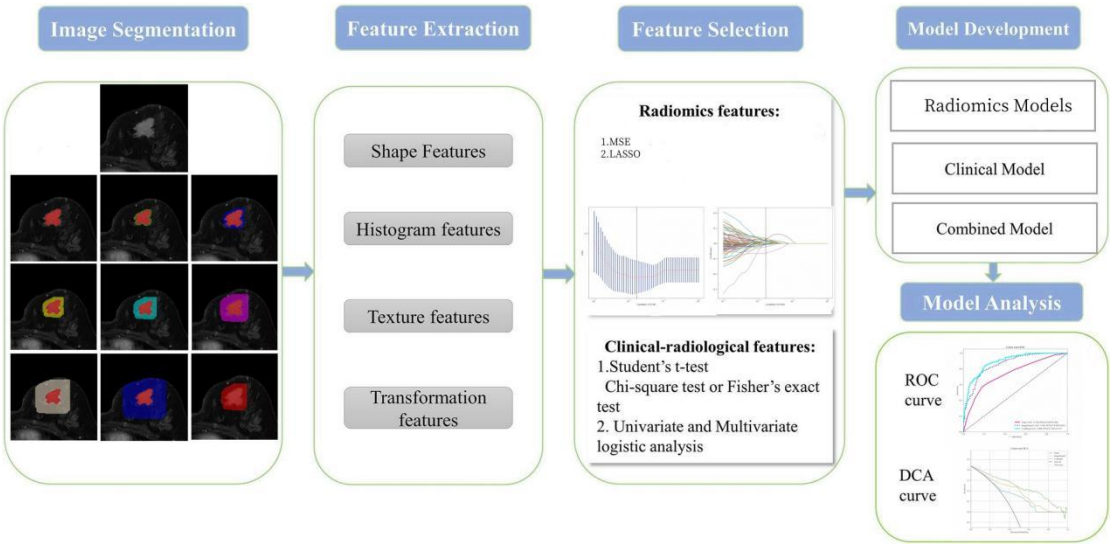


Fig 2. Workflow of this study.

1.4.1 Image Segmentation and Region of Interest (ROI) Definition

ROI Segmentation: Regions of interest (ROIs) were manually delineated using ITK-SNAP software by two experienced radiologists (Reader A and Reader B). Any discrepancies during annotation were resolved by a senior radiologist (Reader C) with over 20 years of experience. Four types of ROIs were defined (Figure 3): - Tumor ROI: The region within the tumor boundary. - Peri ROI: Generated by expanding the Tumor ROI outward by 1, 3, 5, 7, 10, 15, and 20 mm using a Python script, followed by manual trimming of areas extending beyond the breast parenchyma. Feature-level fusion ROI (Tumor+Peri7mm): Features were extracted from both the tumor ROI and the 7mm-peripheral ROI, then the two feature vectors were concatenated. Image-level fusion ROI (ImageFusion7): The tumor ROI and the 7mm-peripheral ROI were merged into a single continuous ROI, from which features were subsequently extracted.

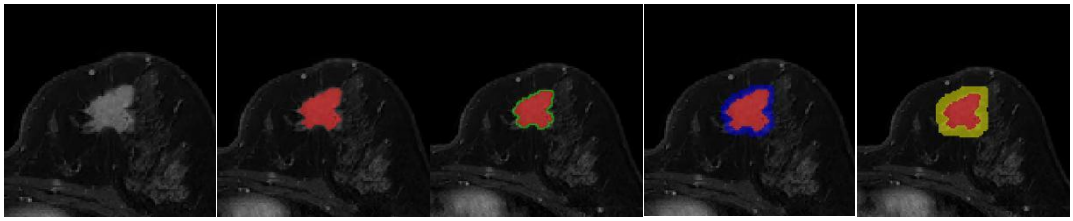


Fig 3a Fig 3b Fig 3c Fig 3d Fig 3e

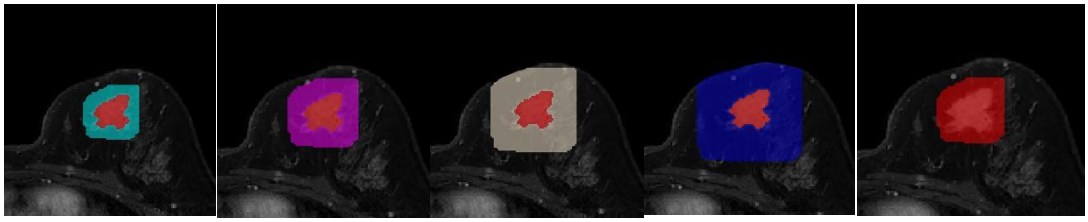


Fig 3f Fig 3g Fig 3h Fig 3i Fig 3j

Figure 3 Schematic diagram of region of interest segmentation in magnetic resonance imaging. Figure a shows the original MRI image of a patient with postoperative pathological diagnosis of breast cancer; Figure b depicts the region of interest

(ROI) within the tumor, delineated along its margins; Figure c shows the peritumoral ROI obtained by expanding 1 mm outward from the tumor margins; Figure d shows the peritumoral ROI obtained by expanding 3 mm outward from the tumor margins; Figure e shows the peritumoral ROI obtained by expanding 5 mm outward from the tumor margins; Figures f - i show the peritumoral regions of interest obtained by expanding 7 mm, 10 mm, 15 mm, and 20 mm outward from the tumor margin, respectively; Figure j shows the fusion region of interest combining the intra-tumoral and 7 mm peritumoral images.

1.4.2 Radiomics Feature Extraction and Selection

Radiomics features were extracted from four ROIs using the open-source Python package PyRadiomics (version 3.7.12; https://pyradiomics.readthedocs.io). Prior to feature extraction, MRI signal intensity from the phase 3 dynamic contrast-enhanced images underwent z-score normalization. Simultaneously, PyRadiomics performed grayscale quantization and resampled the images to isotropic voxels ($1\times1\times1$ mm^3). A total of 1197 features were extracted from both the tumor and each peritumoral ROI. The Tumor+Peri7mm ROI yielded 2394 features (1197×2), while the ImageFusion7 ROI produced 1197 features.

All extracted features were standardized using z-scores and evaluated for statistical significance via t-tests, retaining only those with p-values below 0.05. To mitigate multicollinearity, Pearson correlation coefficients were used to analyze feature associations, eliminating pairs with correlations exceeding 0.9. Within a 10-fold cross-validation framework, Lasso regression was employed to further refine the feature set, determining the optimal regularization parameter λ. This process effectively identified the feature set with the highest predictive value and information content.

1.4.3 Construction of Imageomics Models

The final model was constructed using the same set of machine learning algorithms, ensuring consistency and comparability in the analysis methods applied to both the tumor interior and surrounding regions. Machine learning (ML) models were constructed using five distinct ML classifiers: Support Vector Machine (SVM), Extreme Trees (ET), Extreme Gradient Boosting (XGBoost), Light Gradient Boosting Machine (LightGBM), and Multilayer Perceptron (MLP). For each ROI, the model demonstrating the best and most stable performance across both training and testing cohorts was selected as the final radiomics model for that ROI.

1.4.4 Clinical-Imaging Model and Fusion Model Construction

Univariate logistic regression analysis was performed for all clinical and MRI semantic features. Features with $p < 0.05$ were included in multivariate logistic regression to identify independent predictors of LVI and construct a clinical-imaging model. Based on the selected radiomics features, a radiomics score (Rad-score) was calculated for each patient using linear combination. The fusion model was constructed by incorporating statistically significant clinical-imaging features alongside the Rad-score into multivariate logistic regression.

1.5 Statistical Analysis

Statistical analysis was performed using IBM SPSS Statistics (version 25.0) and

R software (version 4.3.2). Radiomics analysis and machine learning modeling utilized Python (version 3.7.12), supplemented by the statsmodels (0.13.2), PyRadiomics (3.0.1), and scikit-learn (1.0.2) libraries. Continuous variables meeting normal distribution were expressed as mean ± standard deviation and compared using independent samples t-tests. Non-normally distributed variables were expressed as median (interquartile range) and compared using Mann-Whitney U tests. Categorical variables were expressed as counts (percentages) and compared using chi-square tests. Model performance was assessed using area under the receiver operating characteristic (ROC) curve (AUC), sensitivity, specificity, positive predictive value (PPV), negative predictive value (NPV), and accuracy. Model calibration was evaluated using calibration curves and the Hosmer-Lemeshow test. Clinical utility was assessed via decision curve analysis (DCA). Differences in AUC between models were compared using the DeLong test. All tests were performed bilaterally. A p-value < 0.05 was considered statistically significant.

2 Results

2.1 Patient Baseline Characteristics

This study ultimately included 757 patients, comprising 529 cases in the training set and 228 cases in the test set. Among all patients, postoperative pathological examination confirmed LVI in 328 cases (43.33%). The LVI positivity rate was 43.67% (231/529) in the training set and 42.54% (97/228) in the test set, with no significant difference between the two groups (P>0.05). Detailed demographic, clinical-pathological, and MRI semantic features for patients in the training and test sets are presented in Table 1. No statistically significant differences were observed in any baseline characteristics between the two groups (all P > 0.05), indicating balanced and comparable cohort division.

Table1. Baseline analysis of clinical characteristics

feature_name	ALL(n=757)	Training(n=529)	Test(n=228)	p-value
Age (Mean ± SD)	50.17±10.38	50.15±10.56	50.23±9.97	0.840
Menopausalstate, n (%)				0.638
Menopause	314(41.48)	216(40.83)	98(42.98)	
postmenopausal	443(58.52)	313(59.17)	130(57.02)	
Family history of breast cancer, n (%)				0.583
No	689(91.02)	479(90.55)	210(92.11)	
Yes	68(8.98)	50(9.45)	18(7.89)	
Histological Grading, n (%)				0.585
1	90(11.89)	62(11.72)	28(12.28)	
2	462(61.03)	329(62.19)	133(58.33)	
3	205(27.08)	138(26.09)	67(29.39)	
Sentinel lymph node, n (%)				0.740
Yes	297(39.23)	205(38.75)	92(40.35)	
No	460(60.77)	324(61.25)	136(59.65)	
ER, n (%)				0.433
Positive	580(76.62)	410(77.50)	170(74.56)	
Negative	177(23.38)	119(22.50)	58(25.44)	
PR, n (%)				0.210
Positive	511(67.50)	365(69.00)	146(64.04)	
Negative	246(32.50)	164(31.00)	82(35.96)	
HER-2, n (%)				0.863
Positive	201(26.55)	139(26.28)	62(27.19)	

feature_name	ALL(n=757)	Training(n=529)	Test(n=228)	p-value
Negative	556(73.45)	390(73.72)	166(72.81)	
Ki67, n (%)				0.130
High expression	579(76.49)	396(74.86)	183(80.26)	
Low expression	178(23.51)	133(25.14)	45(19.74)	
Molecular Typing, n (%)				0.439
Luminal A	128(16.91)	96(18.15)	32(14.04)	
Luminal B	461(60.90)	320(60.49)	141(61.84)	
HER-2 overexpression	79(10.44)	51(9.64)	28(12.28)	
Triple-negative	89(11.76)	62(11.72)	27(11.84)	
Types of Mammary Gland Tissue, n (%)				0.156
Compact	659(87.05)	454(85.82)	205(89.91)	
Non-compact	98(12.95)	75(14.18)	23(10.09)	
TIC, n (%)				0.968
Ⅰ	81(10.70)	56(10.59)	25(10.96)	
Ⅱ	307(40.55)	216(40.83)	91(39.91)	
Ⅲ	369(48.75)	257(48.58)	112(49.12)	
MRI of axillary lymph nodes, n (%)				0.910
Positive	429(56.67)	301(56.90)	128(56.14)	
Negative	328(43.33)	228(43.10)	100(43.86)	
MRI size, n (%)				1.000
<2 cm	243(32.10)	170(32.14)	73(32.02)	
≥2 cm	514(67.90)	359(67.86)	155(67.98)	

Note: ER estrogen receptor; PR progesterone receptor; HER-2 human epidermal growth factor receptor-2; TIC time signal intensity curve

2.2 Construction of Clinical-Imaging Models

Univariate logistic regression analysis revealed that age, histological grade, sentinel lymph node status, ER, PR, HER-2, Ki67, molecular subtype, breast glandular density, TIC type, and MRI-assessed axillary lymph node status were significantly associated with LVI (all $P < 0.05$). After incorporating these 11 variables into a multivariate logistic regression analysis, results indicated that histological grade (OR=1.671, 95% CI: 1.267 - 2.203, P=0.002), positive sentinel lymph nodes (OR=0.201, 95% CI: 0.143 - 0.283, P<0.001), and TIC type (OR=1.343, 95% CI: 1.070 - 1.685, P=0.033) were independent predictors of LVI. A clinical-imaging model (Clinic model) was constructed based on these factors. Detailed results of univariate and multivariate analyzes are presented in Table 2.

Table 2. Univariable Analysis of clinical features.

feature_name	Single-factor analysis		Multivariate Analysis	
	OR (95% CI)	p_value	OR (95% CI)	p_value
Age	0.994(0.991～0.997)	0.000	0.985(0.970～1.00)	0.110
Menopausalstate	0.906(0.831～0.988)	0.061		
Family history of breast cancer	0.852(0.534～1.358)	0.572		
Histological Grading	0.916(0.859～0.977)	0.026	1.671(1.267～2.203)	0.002
Sentinel lymph node	0.752(0.689～0.821)	0.000	0.201(0.143～0.283)	0.000

ER	0.822(0.735～0.919)	0.004	1.305(0.569～2.989)	0.598
PR	0.842(0.759～0.934)	0.007	1.675(0.956～2.936)	0.131
HER-2	0.860(0.794～0.932)	0.002	1.472(1.004～2.160)	0.097
Ki67	0.794(0.711～0.886)	0.001	0.851(0.507～1.428)	0.607
Molecular Typing	0.901(0.846～0.959)	0.006	0.754(0.465～1.221)	0.336
Types of Mammary Gland Tissue	0.786(0.696～0.887)	0.001	1.052(0.656～1.687)	0.861
TIC	0.908(0.856～0.963)	0.007	1.343(1.070～1.685)	0.033
MRI of axillary lymph nodes	0.812(0.737～0.894)	0.000	1.219(0.877～1.692)	0.322
MRI size	0.916(0.844～0.995)	0.081		

Note: OR denotes odds ratio; CI denotes confidence interval; ER denotes estrogen receptor; PR denotes progesterone receptor; HER-2 denotes human epidermal growth factor receptor-2; TIC denotes time signal intensity curve.

2.3 Construction and Comparison of Imaging Informatics Models

By integrating radiomics with clinical characteristics, we constructed prediction models using five machine learning algorithms based on features selected from four ROI patterns (Tumor, Peri series, Tumor+Peri7mm, ImageFusion7). The AUC performance comparison of each model across different ROIs is detailed in Table 3.

Within the pure tumor (Tumor) ROI, the SVM model demonstrated optimal performance, achieving AUC values of 0.805 and 0.674 on the training and test sets, respectively. Among the peri-tumor (Peri) ROIs at different expansion distances, the Peri-7mm ROI exhibited the best overall prediction performance. In the feature-level fusion (Tumor+Peri7mm) ROI, the MLP model demonstrated the best performance (training set AUC=0.812, test set AUC=0.677). In the image-level fusion (ImageFusion7) ROI, the XGBoost model achieved the best performance due to its advantages in handling small datasets, rapid prototyping, regularization, and interpretability, with training and testing set AUC values of 0.861 and 0.709, respectively. Given that the ImageFusion7 ROI demonstrated the highest AUC value (0.709) in the test set, outperforming all other ROI models, we selected the ImageFusion7 XGBoost model as the outstanding radiomics model (ImageFusion7 model) for subsequent fusion analysis in medical image analysis.

Table 3. AUC of Different Models within Various ROI

AUC	Cohort	SVM	ET	XGBoost	LightGBM	MLP
Tumor	Training	0.805	0.692	0.879	0.792	0.728
Tumor	Testing	0.674	0.634	0.625	0.646	0.679
Peri1mm	Training	0.707	0.640	0.854	0.736	0.640
Peri1mm	Testing	0.562	0.589	0.568	0.584	0.601
Peri3mm	Training	0.666	0.637	0.729	0.710	0.620
Peri3mm	Testing	0.550	0.579	0.608	0.611	0.616
Peri5mm	Training	0.832	0.699	0.890	0.805	0.750

Peri5mm	Testing	0.595	0.608	0.576	0.595	0.607
Peri7mm	Training	0.790	0.715	0.877	0.790	0.728
Peri7mm	Testing	0.649	0.628	0.595	0.615	0.624
Peri10mm	Training	0.791	0.714	0.895	0.810	0.761
Peri10mm	Testing	0.584	0.559	0.585	0.612	0.619
Peri15mm	Training	0.659	0.645	0.796	0.724	0.649
Peri15mm	Testing	0.587	0.590	0.563	0.590	0.583
Peri20mm	Training	0.674	0.657	0.850	0.750	0.634
Peri20mm	Testing	0.563	0.594	0.527	0.563	0.611
Tumor+Peri7mm	Training	0.873	0.703	0.913	0.846	0.812
Tumor+Peri7mm	Testing	0.662	0.623	0.650	0.646	0.677
ImageFusion7	Training	0.817	0.694	0.861	0.822	0.766
ImageFusion7	Testing	0.675	0.692	0.709	0.695	0.680

Note: AUC area under receiver operating characteristic curve, SVM Support Vector Machines, ET extra trees, , XGBoost eXtreme Gradient Boosting, LightGBM Light Gradient Boosting Machine, MLP Multi-layer Perceptron

2.4 Model Performance Evaluation and Comparison

The system evaluated and compared the performance of the clinical-imaging model (Clinic), the optimal radiomics model (ImageFusion7), and the combined model integrating both (Combined). Diagnostic performance metrics for each model are presented in Table 4, with corresponding ROC curves shown in Figure 4.

In the training set, the AUC (95% CI) values for the Combined model, Clinic model, and ImageFusion7 model were 0.890 (0.863–0.917), 0.738 (0.695–0.780), and 0.861 (0.830–0.891), respectively. In the test set, the AUC values for the three models were 0.776 (0.714 – 0.838), 0.749 (0.683 – 0.814), and 0.709 (0.641 – 0.777), respectively. The Combined model achieved the highest AUC values in both the training and test sets, indicating that integrating clinical-imaging features with radiomics features effectively enhances the model's predictive capability for LVI.

Table 4. Metrics for Different Signatures

Signature	Cohort	Accuracy	AUC	95% CI	Sensitivity	Specificity	PPV	NPV
Clinic	Training	0.711	0.738	0.6949 – 0.7802	0.567	0.822	0.712	0.710
Clinic	Testing	0.750	0.749	0.6830 – 0.8141	0.680	0.802	0.717	0.772
ImageFusion7	Training	0.794	0.861	0.8302 – 0.8914	0.775	0.809	0.758	0.823
ImageFusion7	Testing	0.658	0.709	0.6407 – 0.7768	0.732	0.603	0.577	0.752
Combined	Training	0.815	0.890	0.8629 – 0.9165	0.840	0.795	0.761	0.865
Combined	Testing	0.759	0.776	0.7140 – 0.8375	0.619	0.863	0.769	0.753

Note: AUC – Area Under the Receiver Operating Characteristic Curve; PPV – Positive Predictive Value; NPV – Negative Predictive Value

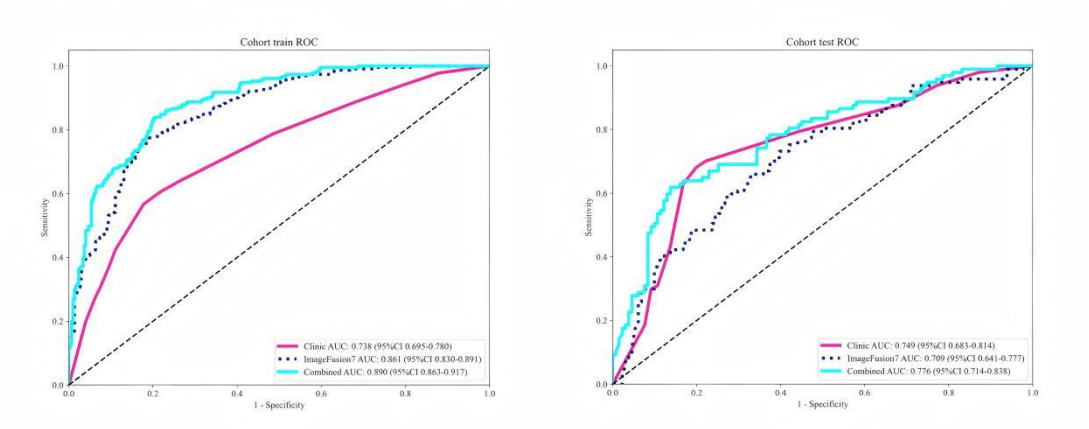


Fig 4. ROC of Different Signatures in Different Cohorts

2.5 Model Calibration Accuracy and Clinical Utility

According to the results of the Hosmer-Lemeshow test, the predicted probabilities of the Combined model in the test set show good consistency with the actual observed outcomes (Figure 5), indicating that the model exhibits good calibration.

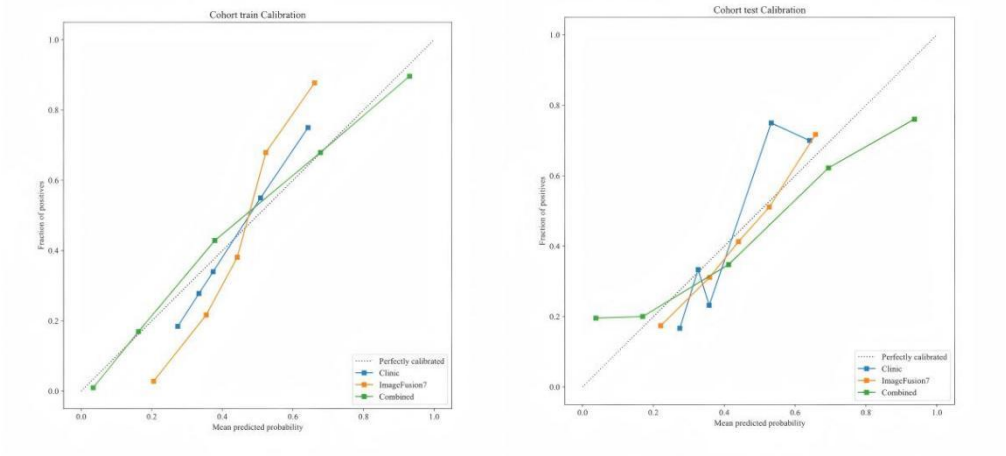


Fig 5. Calibration curves of different signatures for the test cohort.

DeLong Test: By applying DeLong's test in R, we conducted statistical significance tests on the training and testing datasets to evaluate performance differences among models. Results indicate that our integrated model statistically outperforms both the traditional omics model and the peritumoral region model (Figure 6), though the improvement over the MIL model is not statistically significant. This may be attributed to the limited incremental information gain provided by integrating omics data with the MIL model.

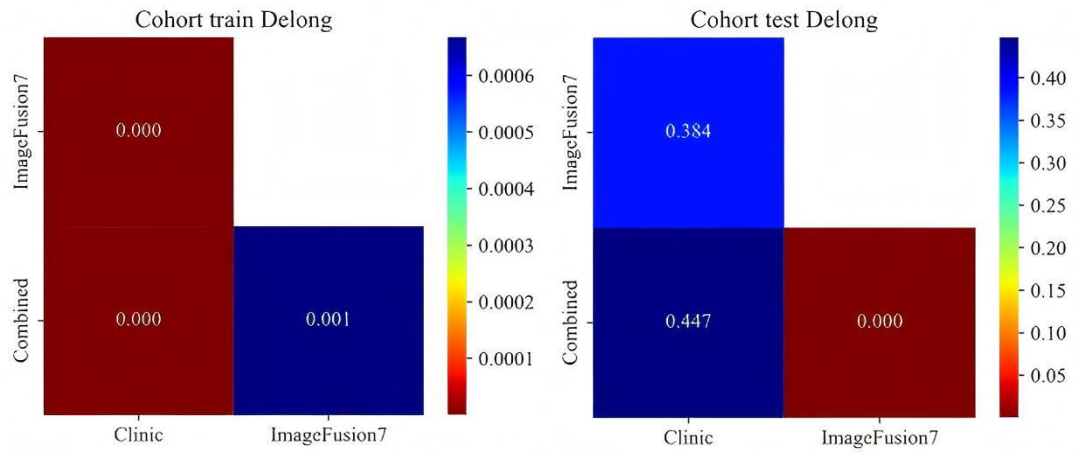


Figure 6. DeLong test results for different signatures.

Clinical Use

As shown in Figure 7, decision curve analysis (DCA) of the training and testing sets reveals the significant advantage of our fusion model in predicting probabilities. DCA evaluates the model's net benefit—the number of true positive patients it can identify—reflecting its efficiency. A higher net benefit indicates greater model efficiency. Furthermore, compared to other features, this model consistently demonstrates higher net benefit potential, fully highlighting its effectiveness. The predictive nomogram integrates clinical and pathological factors with ImageFusion7—a fusion of intra-tumoral and peritumoral regions within a 7 mm margin based on dynamic contrast-enhanced MRI (see Figure 8).

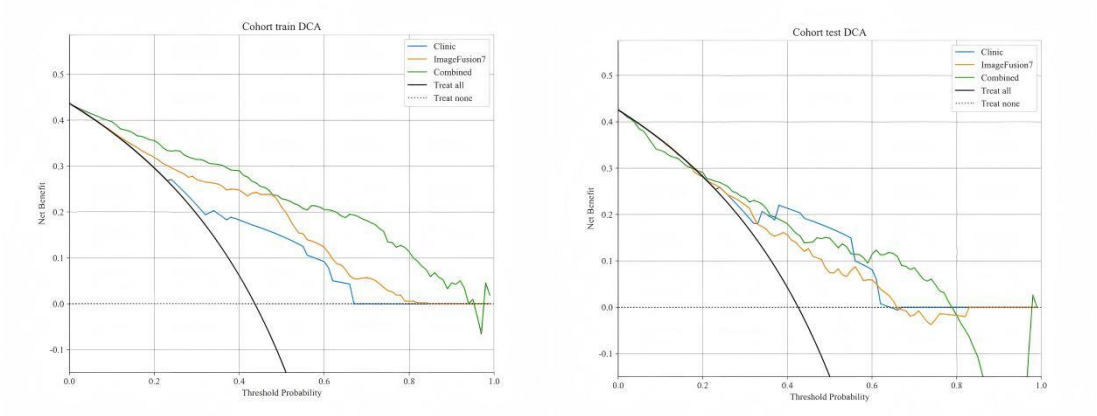


Fig 7. Different signatures' decision curve on test cohort.

2.6 Construction of the Prediction Column Chart

To further achieve individualized prediction, we integrated clinically and radiologically significant features with independent predictive value from multivariate analysis (histological grade, sentinel lymph node status, and TIC type) with the radiomics score (Rad-score) from the ImageFusion7 model. This resulted in a visual predictive nomogram (Figure 8). This nomogram enables intuitive estimation of the probability of lymphovascular invasion (LVI) in breast cancer patients.

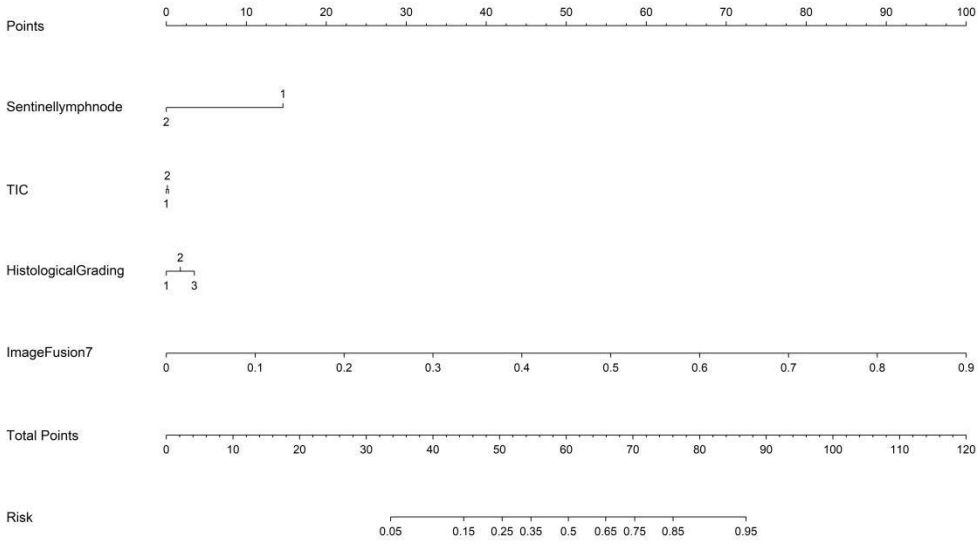


Fig 8. A predictive nomogram integrating clinical and pathological factors with a 7 mm image fusion zone encompassing both the tumor interior and peritumoral region based on dynamic contrast-enhanced MRI (ImageFusion7).

3 Discussions

This multicenter DCE-MRI radiomics study systematically compared the predictive value of different intra-tumoral, peritumoral, and intra-peritumoral image fusion models for breast cancer lymphovascular invasion (LVI) status. Key findings include: (1) Radiomics models based on ImageFusion7 (7mm intra- and peritumoral image fusion) ROIs demonstrated superior predictive performance compared to intra- or peritumoral models alone; (2) A clinical-imaging model incorporating histological grade, sentinel lymph node status, and tumor-infiltrating carcinoma (TIC) type demonstrated stable predictive capability; (3) A combined model integrating clinical-imaging and radiomics features achieved optimal discriminatory performance (AUC=0.890 in training set, AUC=0.776 in validation set) and clinical net benefit, indicating significant potential for clinical application. These findings indicate that peritumoral radiomics features provide incremental predictive value beyond traditional intratumoral models. This discovery fills a gap in research on the optimal peritumoral region for breast cancer LVI status prediction, offering an intuitive and non-invasive approach for future LVI status forecasting.

3.1 The Value of Peritumoral Radiomics in the Tumor Microenvironment

Previous studies have predominantly focused on the intratumoral region, whereas this research further reveals the significant biological information contained within the peritumoral area. The interactions between tumor cells and the peritumoral microenvironment profoundly influence tumor progression and metastasis. Combined analysis can provide complementary information, thereby enhancing the predictive capability of models [19]. Previous studies have confirmed that incorporating the tumor periphery enhances the efficacy of sentinel lymph node

prediction [20-21], potentially due to its analysis of heterogeneities such as marginal invasion. At the microscopic level, the region surrounding the lesion contains important areas including diverse immune cells and abnormal blood vessels. Immune cell distribution and vascular abnormalities may promote tumor progression and metastasis [22-23]. Regarding breast cancer LVI status, margin heterogeneity warrants further investigation. Kazerouni et al. [24] similarly identified correlations between tumor microenvironment and clinical treatment efficacy using DCE-MRI imaging. Thus, in-depth analysis of this region in the present study may aid in predicting disease-related biomarkers, providing crucial reference for clinical decision-making.

3.2 Correlation Analysis Between Clinical Pathological Characteristics and LVI

In this study, the distributions of most clinical and imaging features showed no significant differences between the training and testing sets, indicating balanced dataset partitioning without apparent bias or overfitting.

Univariate analysis revealed that age, histological grade, sentinel lymph node status, ER, PR, HER-2, Ki-67, molecular subtype, breast glandular density, TIC type, and MRI axillary lymph node status were all significantly associated with LVI (all $P < 0.05$). Among these, histological grade (AUC = 0.916), molecular subtype (AUC = 0.901), and TIC type (AUC = 0.908) demonstrated strong discriminatory ability in the univariate model. Although age demonstrated a high univariate AUC (0.994), its narrow confidence interval (0.991 - 0.997) suggested potential model specificity. The univariate AUC for sentinel lymph node status was relatively low (0.752) with a wide confidence interval, indicating uncertainty when used as a single predictor.

Multivariate logistic regression analysis ultimately identified high histological grade, positive sentinel lymph nodes, and Type III (effluent) tumor-initiating cells (TICs) as independent predictors of lymphovascular invasion (LVI). This aligns with findings by Nishimura et al. [25], who reported that LVI is more prevalent in tumors with higher histological grades, suggesting that poor cellular differentiation and active proliferation correlate with increased invasiveness. Furthermore, our findings support LVI as a risk factor for sentinel lymph node metastasis, aligning with the conclusions of Ning et al. [26]. Type III TIC reflects high tumor vascular permeability and complex hemodynamics, closely associated with an aggressive phenotype and increased angiogenesis [27]. These indicators are readily obtainable from routine pathology and MRI, endowing the clinical-imaging model with both practicality and predictive efficacy.

3.3 Correlation between Intratumoral and Peritumoral Imaging Features and Lymphovascular Invasion

In recent years, radiomics has emerged as a research hotspot for predicting LVI. While previous studies primarily focused on intra-tumoral features [28-30], this study extracted radiomic features based on intra-tumoral, peritumoral, intra-tumoral + peritumoral, and intra-tumoral-peritumoral image fusion MRI. By incorporating peritumoral analysis, predictive performance was further enhanced. Results indicate that the ImageFusion7 radiomics model, integrating intra-tumoral and peri-tumoral

information, demonstrated the highest predictive accuracy for LVI status in breast cancer patients, suggesting that combining these domains provides a more comprehensive characterization of tumor heterogeneity. Research indicates that over 85% of microvascular invasion occurs in the peritumoral region [31], and peritumoral radiomics features are crucial for breast cancer diagnosis, prognosis prediction, and treatment response evaluation [32-33]. The peritumoral area contains microenvironmental information closely related to angiogenesis and immune responses, which are directly linked to the mechanisms underlying LVI development. Jiang et al. [34] demonstrated that integrating intra-tumoral and peri-tumoral features from DCE-MRI and DWI significantly enhances LVI diagnostic accuracy (AUC 0.870), consistent with the findings of this study.

In this study, AUC analysis revealed markedly different performance patterns of various features across the training and testing cohorts. Within the training cohort, the combined model features achieved the highest AUC value (0.890), followed by ImageFusion7 (AUC = 0.861) and clinical features (AUC = 0.738), indicating superior discriminative capability of the integrated approach. The 95% confidence interval (CI) further validated this ranking: the combined feature's CI was the narrowest (0.8629 - 0.9165), indicating superior reliability compared to ImageFusion7 (CI: 0.8302 - 0.8914) and clinical features (CI: 0.6949 - 0.7802). In the test cohort, the composite feature maintained the highest AUC (0.776) but showed reduced performance compared to the training cohort; clinical features (0.749) and ImageFusion7 (0.709) exhibited lower AUC values yet remained comparable. The confidence intervals (CI) were wider in the test cohort, particularly for ImageFusion7 (0.6407 - 0.7768), indicating reduced generalization capability compared to the training data. The final fusion model, constructed using intra-tumor and peri-tumor radiomics features (extracted as a single ROI), yielded higher predictive values than other radiomics models—a finding uncommon in previous studies [35-37].

These findings demonstrate that the combined model consistently outperformed single modalities (clinical features and ImageFusion7) in distinguishing the target pathology, as evidenced by higher AUC values and narrower confidence intervals across both cohorts. However, a decline in performance was observed for all features in the test cohort, underscoring the importance of validating models on independent datasets to assess their practical applicability. Clinical features exhibited relatively stable AUC values (0.738 - 0.749) across cohorts, indicating moderate and consistent diagnostic utility. Conversely, the lower AUC (0.709) of image fusion features in the test cohort raises concerns about their robustness. Overall, the combined features demonstrate a highly promising balance in sensitivity, specificity, and generalization capability, making them an ideal candidate for clinical application. Nevertheless, further optimization and external validation are still required.

3.4 Limitations of this study

Despite employing a multicenter design to enhance generalizability, the sample size still has room for expansion. Furthermore, as a retrospective study, the current

research may be subject to data loss and selection bias. To ensure the universal applicability of findings, future studies should consider adopting prospective designs, such as prospective randomized controlled trials or cohort studies, to further validate results and reduce bias. Second, manual lesion segmentation employed in this study is a time-consuming and somewhat subjective process. Future exploration of automated or semi-automated segmentation algorithms could enhance efficiency and standardization [38-40]. Third, this study relied solely on DCE-MRI sequences. Integrating multi-parametric MRI (e.g., DWI, T2 mapping) or even multimodal imaging data in future research may further unlock predictive potential.

In summary, this study constructed and validated a fusion model based on multicenter DCE-MRI that effectively predicts the LVI status of breast cancer preoperatively. By comparing different peritumoral ranges and feature fusion methods, the ImageFusion7 radiomics model demonstrated optimal performance. Furthermore, integrating clinical features significantly enhanced its predictive capability. The predictive capability of peritumoral radiomics demonstrates significant incremental value compared to both intra-tumoral radiomics assessment alone and clinical feature models. This model provides a reliable tool for non-invasive, individualized preoperative assessment of LVI risk and holds potential for clinical translation.

Acknowledgments

Not applicable.

Authors contributions

H.L, Y. Z (Yihui Zeng), Y. Z (Yan Zhang). designed the study.H.L .performed the majority of the experiments.Y.Z(Yihui Zeng).provided assistance for the experiments and data analysis.Q.X,J.T.wrote the draft of the manuscript, and revised the manuscript.Y.Z(Yihui Zeng). confirm the authenticity of all the raw data. All authors read and approved the final version of the manuscript.

Funding

No

Data availability

Due to the sensitive nature of the patient imaging and clinical data collected for this study, the data are not publicly available. However, anonymized data may be provided by the corresponding author upon reasonable request and with appropriate institutional ethics approval.

Declarations

Ethics approval and consent to participate

This retrospective study was approved by the Medical Ethics Committee of Guangdong Women and Children Hospital (Approval No.: Guangdong Women and Children Hospital Medical Ethics No. [20261015]) and the Scientific Research Ethics Committee of the First Affiliated Hospital of Jinan University (Approval No.: KY-2026-109). The study

was conducted in accordance with the principles of the Declaration of Helsinki. The requirement for informed consent was waived by both ethics committees due to the retrospective nature of the study.

Consent for publication

Not applicable.

Competing interests

The authors declare no competing interests.

Author details

Department of Radiology, Guangdong Women and Children Hospital, Guangzhou 511400, China

References

[1] Siegel RL, Giaquinto AN, Jemal A. Cancer statistics, 2024. CA Cancer J Clin. 2024 Jan-Feb;74(1):12-49. doi: 10.3322/caac.21820. Epub 2024 Jan 17. Erratum in: CA Cancer J Clin. 2024 Mar-Apr;74(2):203.
[2] Kim J, Harper A, McCormack V,et al. Global patterns and trends in breast cancer incidence and mortality across 185 countries. Nat Med. 2025 Apr;31(4):1154-1162.
[3] Rakha EA, Abbas A, Pinto Ahumada P,et al. Diagnostic concordance of reporting lymphovascular invasion in breast cancer. J Clin Pathol. 2018 Sep;71(9):802-805.
[4] Corachea AJM, Ferrer RJE, Ty LPB,et al. Lymphovascular Invasion Is Associated With Doxorubicin Resistance in Breast Cancer. Lab Invest. 2025 May;105(5):104115.
[5] Null JL, Kim DJ, McCann JV,et al. Periostin+ Stromal Cells Guide Lymphovascular Invasion by Cancer Cells. Cancer Res. 2023 Jul 5;83(13):2105-2122.
[6] Zhong YM, Tong F, Shen J. Lympho-vascular invasion impacts the prognosis in breast-conserving surgery: a systematic review and meta-analysis. BMC Cancer. 2022 Jan 25;22(1):102.
[7] Houvenaeghel G, Cohen M, Classe JM,et al. Lymphovascular invasion has a significant prognostic impact in patients with early breast cancer, results from a large, national, multicenter, retrospective cohort study. ESMO Open. 2021 Dec;6(6):100316.
[8] Yang X, Xu M, Xia Y,et al. Plasma-derived exosomal human epidermal growth factor receptor 2 (HER2) protein for distinguishing breast cancer from benign breast disease and assessing the efficacy of neoadjuvant therapy. Transl Cancer Res. 2025 May 30;14(5):3186-3200.
[9] Wu Q, Zhu M, Xie H,et al. Dynamic Evolution of Vascular Features Based on Magnetic Resonance Imaging to Predict Pathological Response, Patterns of Recurrence and Survival Outcomes in Breast Cancer Neoadjuvant Chemotherapy. Curr Oncol. 2025 Jun 13;32(6):350.
[10] Wang Y, Chen X, Pu H,et al. Roles of DWI and T2-weighted MRI volumetry in the evaluation of lymph node metastasis and lymphovascular invasion of stage IB-IIA cervical cancer. Clin Radiol. 2022 Mar;77(3):224-230.

[11] Choi EJ, Youk JH, Choi H,et al. Dynamic contrast-enhanced and diffusion-weighted MRI of invasive breast cancer for the prediction of sentinel lymph node status. J Magn Reson Imaging. 2020 Feb;51(2):615-626.
[12] Qi YJ, Su GH, You C,et al. Radiomics in breast cancer: Current advances and future directions. Cell Rep Med. 2024 Sep 17;5(9):101719.
[13] Zhang Z, Lan H, Zhao S. Analysis of the Value of Quantitative Features in Multimodal MRI Images to Construct a Radio-Omics Model for Breast Cancer Diagnosis. Breast Cancer (Dove Med Press). 2024 Jun 11;16:305-318.
[14] Wang H, Chen W, Jiang S,et al. Intra- and peritumoral radiomics features based on multicenter automatic breast volume scanner for noninvasive and preoperative prediction of HER2 status in breast cancer: a model ensemble research. Sci Rep. 2024 Feb 29;14(1):5020.
[15] Panthi B, Mohamed RM, Adrada BE,et al. Longitudinal dynamic contrast-enhanced MRI radiomic models for early prediction of response to neoadjuvant systemic therapy in triple-negative breast cancer. Front Oncol. 2023 Oct 24;13:1264259.
[16] Huang Z, Mo S, Wu H,et al. Optimizing breast cancer diagnosis with photoacoustic imaging: An analysis of intratumoral and peritumoral radiomics. Photoacoustics. 2024 Apr 9;38:100606.
[17] Ding J, Chen S, Serrano Sosa M,et al. Optimizing the Peritumoral Region Size in Radiomics Analysis for Sentinel Lymph Node Status Prediction in Breast Cancer. Acad Radiol. 2022 Jan;29 Suppl 1(Suppl 1):S223-S228.
[18] GOLDHIRSCH A, WINER EP, COATES AS,et al. Personalizing the treatment of women with early breast cancer: highlights of the St Gallen International Expert Consensus on the Primary Therapy of Early Breast Cancer 2013[J]. Ann Oncol. 2013,24(9):2206-23.
[19] Li X, Fang J, Wang F,et al. Prediction of HER2 expression in breast cancer patients based on multi-parametric MRI intratumoral and peritumoral radiomics features combined with clinical and imaging indicators. Front Oncol. 2025 Jun 9;15:1531553.
[20] Lin F, Li Q, Wang Z,et al. Intratumoral and peritumoral radiomics for preoperatively predicting the axillary non-sentinel lymph node metastasis in breast cancer on the basis of contrast-enhanced mammography: a multicenter study. Br J Radiol. 2023 Mar;96(1143):20220068.
[21] Ding J, Chen S, Serrano Sosa M,et al. Optimizing the Peritumoral Region Size in Radiomics Analysis for Sentinel Lymph Node Status Prediction in Breast Cancer. Acad Radiol. 2022 Jan;29 Suppl 1(Suppl 1):S223-S228.
[22] Akinpelu A, Akinsipe T, Avila LA,et al. The impact of tumor microenvironment: unraveling the role of physical cues in breast cancer progression. Cancer Metastasis Rev. 2024 Jun;43(2):823-844.
[23] Liu Y, Li X, Zhu L,et al. Preoperative Prediction of Axillary Lymph Node Metastasis in Breast Cancer Based on Intratumoral and Peritumoral DCE-MRI Radiomics Nomogram. Contrast Media Mol Imaging. 2022 Aug 18;2022:6729473.

[24] Kazerouni AS, Peterson LM, Jenkins I,et al. Multimodal prediction of neoadjuvant treatment outcome by serial FDG PET and MRI in women with locally advanced breast cancer. Breast Cancer Res. 2023 Nov 9;25(1):138.
[25] Nishimura R, Osako T, Okumura Y,et al. An evaluation of lymphovascular invasion in relation to biology and prognosis according to subtypes in invasive breast cancer. Oncol Lett. 2022 Jun 7;24(2):245.
[26] Ning Ning. Preoperative Prediction of Vascular Invasion in Young Breast Cancer Using a Nomogram Based on Multimodal MRI Intratumoral and Peritumoral Radiomics [D]. Dalian Medical University, 2024.
[27] Li Q, Xie F, Jiang X,et al. Histogram analysis of relaxometry from synthetic MRI for differentiation of breast BI-RADS 4 non-mass enhancement lesions. BMC Med Imaging. 2025 Oct 13;25(1):408.
[28] Niu R, Chen Z, Li Y,et al. A Novel Deep Learning Radiomics Nomogram Integrating B-Mode Ultrasound and Contrast-Enhanced Ultrasound for Preoperative Prediction of Lymphovascular Invasion in Invasive Breast Cancer. Ultrasound Med Biol. 2025 Nov;51(11):1945-1952.
[29] Peng L, Niu J, Huang G,et al. Noninvasive prediction of lymphovascular invasion in rectal cancer without lymph node metastasis using a SHAP-interpretable combined model integrating MRI radiomics features and clinical immune-inflammatory biomarkers: a bicenter study. Cancer Imaging. 2025 Oct 30;25(1):123.
[30] Nijiati M, Aihaiti D, Huojia A,et al. MRI-Based Radiomics for Preoperative Prediction of Lymphovascular Invasion in Patients With Invasive Breast Cancer. Front Oncol. 2022 Jun 6;12:876624.
[31] Dong X, Jia X, Zhang W,et al. Interpretable and generalizable deep learning model for preoperative assessment of microvascular invasion and outcome in hepatocellular carcinoma based on MRI: a multicenter study. Insights Imaging. 2025 Jul 3;16(1):151.
[32] Zhang S, Shao H, Li W,et al. Intra- and peritumoral radiomics for predicting malignant BiRADS category 4 breast lesions on contrast-enhanced spectral mammography: a multicenter study. Eur Radiol. 2023 Aug;33(8):5411-5422.
[33] Wang J, Gao W, Lu M,et al. Development of an interpretable machine learning model for Ki-67 prediction in breast cancer using intratumoral and peritumoral ultrasound radiomics features. Front Oncol. 2023 Nov 17;13:1290313.
[34] Jiang W, Meng R, Cheng Y,et al. Intra- and Peritumoral Based Radiomics for Assessment of Lymphovascular Invasion in Invasive Breast Cancer. J Magn Reson Imaging. 2024 Feb;59(2):613-625.
[35] Zhu Y, Zhang S, Wei W,et al. Intra- and peritumoral radiomics nomogram based on DCE-MRI for the early prediction of pathological complete response to neoadjuvant chemotherapy in breast cancer. Front Oncol. 2025 Jun 4;15:1561599.
[36] Zhao Q, Zhang H, Xing W. Integrating Peritumoral and Intratumoral Radiomics with Deep Learning for Preoperative Prediction of Lymphovascular Invasion in Invasive Breast Cancer Using DCE-MRI. Technol Cancer Res Treat. 2025 Jan-Dec;24:15330338251374945.

[37] Zhou YH, Liu Y, Zhang X,et al. Dual-phase contrast-enhanced CT-based intratumoral and peritumoral radiomics for preoperative prediction of lymphovascular invasion in gastric cancer. BMC Med Imaging. 2025 Feb 10;25(1):43.
[38] Sanabria-Diaz G, Cagol A, Lu PJ,et al. Advanced MRI Measures of Myelin and Axon Volume Identify Repair in Multiple Sclerosis. Ann Neurol. 2024 Oct 10;97(1):134-48.
[39] Coll L, Pareto D, Aparicio-Serrano F,et al. Deep learning to predict progression independent of relapse activity at a first demyelinating event. Brain Commun. 2025 Jul 4;7(4):fcaf243.
[40] Yin J, Liu L, Luo X,et al. MHAU-Net: a multi-scale hybrid attention U-shaped network for the segmentation of MRI breast tumors. Quant Imaging Med Surg. 2025 May 1;15(5):4758-4773.